
QIVC-NET: QUANTUM-INSPIRED VARIATIONAL CONVOLUTIONAL NETWORK, WITH APPLICATION TO BIOSIGNAL CLASSIFICATION

Amin Golnari *
Faculty of Computer Science
Chemnitz University of Technology
Chemnitz, Germany
amingolnarii@gmail.com

Jamileh Yousefi 
Shannon School of Business
Cape Breton University
Sydney, NS, Canada
jamileh_yousefi@cbu.ca

Reza Moheimani 
Faculty of Computer Science
Chemnitz University of Technology
Chemnitz, Germany
rezamoheiman@gmail.com

Saeid Sanei 
Department of Electrical and Electronic Engineering, Imperial College London
College of Engineering and Computer Science, VinUniversity
London, UK / Hanoi, Vietnam
s.sanei@imperial.ac.uk
saeid.s@vinuni.edu.vn

ABSTRACT

This work introduces the quantum-inspired variational convolution (QiVC) framework, a novel learning paradigm that integrates principles of probabilistic inference, variational optimization, and quantum-inspired transformations within convolutional architectures. The central innovation of QiVC lies in its quantum-inspired rotated ensemble (QiRE) mechanism. QiRE performs differentiable low-dimensional subspace rotations of convolutional weights, analogously to quantum state evolution. This approach enables structured uncertainty modeling while preserving the intrinsic geometry of the parameter space, resulting in more expressive, stable, and uncertainty-aware representations. To demonstrate its practical potential, the concept is instantiated in a QiVC-based convolutional network (QiVC-Net) and evaluated in the context of biosignal classification, focusing on phonocardiogram (PCG) recordings, a challenging domain characterized by high noise, inter-subject variability, and often imbalanced data. The proposed QiVC-Net integrates an architecture in which the QiVC layer does not introduce additional parameters, instead performing an ensemble rotation of the convolutional weights through a structured mechanism ensuring robustness without added highly computational burden. Experiments on two benchmark datasets, PhysioNet CinC 2016 and PhysioNet CirCor DigiScope 2022, show that QiVC-Net achieves state-of-the-art performance, reaching accuracies of 97.84% and 97.89%, respectively. These findings highlight the versatility of the QiVC framework and its promise for advancing uncertainty-aware modeling in real-world biomedical signal analysis. The implementation of the QiVConv layer is openly available in GitHub.

Keywords Cardiovascular Signal Analysis · Coronary Artery Disease · Phonocardiogram Classification · Probabilistic Deep Learning · Quantum-Inspired Weight Ensembling · Variational CNN

1 Introduction

Probabilistic deep learning has emerged as a critical direction for advancing model reliability, interpretability, and robustness in real-world decision-making settings. Unlike deterministic neural networks that produce single-point predictions, probabilistic models explicitly account for uncertainty, allowing them to represent ambiguity in both

*Corresponding author: Amin Golnari <amingolnarii@gmail.com>

parameters and observations [1,2]. However, many existing Bayesian deep learning frameworks approximate uncertainty through simplistic isotropic noise models or mean-field assumptions [3], which fail to capture the structured and geometry-aware variability present in high-dimensional parameter spaces. As a result, uncertainty estimates often become poorly calibrated and unstable under distributional shifts, limiting their usefulness in safety-critical applications [4,5].

To address these limitations, the quantum-inspired variational convolution (QiVC) framework is introduced, incorporating a geometric and variational treatment of uncertainty directly within convolutional layers. The central innovation of this framework is the quantum-inspired rotated ensemble (QiRE) mechanism, which applies differentiable, low-dimensional subspace rotations to convolutional kernels. This operation is inspired by unitary evolution in quantum systems and preserves the intrinsic geometry and norm of the weight space [6]. By enforcing coherent structure in stochastic perturbations, the QiVC layer enables richer uncertainty representation while avoiding the instability and expressiveness limitations of isotropic or unstructured Gaussian perturbations. Importantly, QiVC does not introduce additional learnable parameters; instead, it structurally re-parameterizes the convolutional filters to generate expressive, probabilistically grounded ensembles with minimal computational overhead.

Building on prior developments in quantum-inspired neural architectures [7,8] and functional variational inference [9], QiVC provides a principled approach for embedding uncertainty directly into the model’s functional representation. By unifying variational learning with geometry-preserving transformations, it bridges Bayesian inference with structured ensemble modeling, yielding stable and interpretable feature representations suitable for decision-critical domains.

In this work, the QiVC framework is instantiated within a convolutional network, referred to as QiVC-Net, and its effectiveness is evaluated in the context of phonocardiogram (PCG) classification. PCG signal analysis plays a vital role in computer-aided auscultation and early detection of cardiovascular diseases. Heart sound recordings provide clinically significant diagnostic cues, yet their interpretation is complicated by low signal-to-noise ratios, high inter-patient variability, and environmental artifacts typical of real-world settings [10]. Recent advances in deep learning have improved PCG classification performance through CNNs, RNNs, transformers, and hybrid models [11, 12]. Nevertheless, persistent challenges remain regarding robustness, interpretability, dataset imbalance, and the lack of reliable uncertainty quantification [13–15].

To enhance temporal coherence and robustness to physiological variability, QiVC-Net further incorporates a reversal fusion residual (RFR) block that models bidirectional temporal dependencies in PCG recordings. This combination of geometry-aware probabilistic convolution and temporal symmetry makes QiVC-Net well-suited for biosignal analysis under noisy and heterogeneous conditions.

The main contributions of this work are summarized as follows:

- **QiVConv layer:** A probabilistic convolutional layer introducing norm-preserving subspace rotations that enhance uncertainty calibration while maintaining expressive kernel structure.
- **QiRE sampling:** A structured stochastic perturbation mechanism that performs differentiable unitary-inspired rotations of convolutional weights, enabling Bayesian-like inference without complex-valued arithmetic.
- **Uncertainty-aware dual-path architecture:** Integration of QiVConv with a RFR block to capture bidirectional temporal dynamics in PCG signals without adding extra learnable parameters.
- **Clinically aligned design:** A computationally efficient and interpretable framework unifying uncertainty quantification, robustness to signal variation, and temporal coherence for reliable PCG-based decision support.

2 Literature Review

2.1 Architectural and Probabilistic Modeling Advances

The focus of recent research has been to improve the robustness to noise and recording variability, strengthening temporal feature modeling, and developing more reliable uncertainty estimation in PCG classification. Barnawi et al. [16] introduced a minimal preprocessing strategy combined with CNN fine-tuning to improve efficiency. Riaz et al. [17] developed a portable embedded system leveraging hand-crafted spectral and temporal features. Bidirectional recurrent architectures [18] have been shown to effectively capture the inherent temporal symmetry of PCG signals [19], while hybrid CNN–BiLSTM ensembles improve robustness under noisy conditions [20]. Phoemsuk and Abolghasemi [21] further highlighted the importance of signal-quality-aware preprocessing within lightweight one-dimensional CNNs for reliable cardiovascular disease detection.

On the probabilistic side, dropout-based inference [1] and Bayes by Backprop [22] introduced scalable uncertainty modeling, and later approaches such as multiplicative normalizing flows [23] improved posterior expressiveness.

However, these frameworks typically overlook the geometric dependencies among kernel parameters, where naive noise injection may violate intrinsic correlations and distort the weight space geometry. Consequently, existing Bayesian formulations often misrepresent epistemic uncertainty in structured signals like PCG.

2.2 Phonocardiogram Classification

Over the past decade, PCG classification has progressed from model-driven to data-driven feature engineering toward hybrid and fully deep learning frameworks, with increasing attention to label-efficient, resource-constrained, and murmur-aware designs. Tuncer et al. [24] introduced a graph-theoretic framework combining Petersen graph patterns (PGP), tent energy pooling (TEP), and iterative neighborhood component analysis (INCA) to extract compact yet discriminative features from PCG recordings. Chen et al. [25] applied a three-layer deep neural network to mel-frequency cepstral coefficient (MFCC) super-vectors to identify S1 and S2 heart-sound events directly from acoustic data, demonstrating the feasibility of purely audio-based deep models for event-aware classification without explicit temporal priors.

As research advanced, two-dimensional spectrogram representations became a preferred input format for discriminative learning. Karhade et al. [26] transformed PCG signals into polynomial-chirplet spectrograms and classified them using a custom CNN. Khan et al. [27] developed Cardi-Net, a deep residual CNN designed for high-resolution power spectrograms with extensive augmentation to enhance robustness. Joshi et al. [28] integrated one-dimensional and two-dimensional CNNs into a handheld, three-dimensional printed stethoscope, enabling on-device PCG analysis with minimal latency.

Although spectrogram-based models offer strong representational capacity, they often require large annotated datasets. Transfer learning has been widely adopted to address this challenge. Hettiarachchi et al. [29] proposed a dual-input architecture that fuses separately pre-trained CNN models using PCG and electrocardiogram (ECG), enabling effective classification from limited synchronized recordings. Almanifi et al. [30] demonstrated the adaptation of image-domain pre-trained models to PCG spectrograms for transfer learning. Nehary and Rajan [31] explored positive-unlabelled learning for situations with incomplete annotations, using CNN ensembles with self-attention to separate known normal cycles from unlabeled abnormal ones.

To better detect murmurs in raw recordings, several studies have inserted explicit signal separation stages before classification. The foundational principle of isolating crucial cyclic components was demonstrated by Sanei et al. [32], who proposed a singular spectrum analysis-based adaptive line enhancer (SSA-ALE) to robustly separate quasi-periodic signals, such as heart murmurs, from noise by exploiting the full eigen-spectrum of the SSA embedding matrix. Building on this, Qi and Sanei [33] later developed a two-stage murmur isolation method combining constrained SSA with wavelet refinement, guided by acoustic statistics such as zero-crossing rate and kurtosis. This approach enhances the downstream classification and can reduce computational load. In parallel, Ma et al. [34] applied self-supervised pretraining on large unlabeled PCG corpora to create efficient one-dimensional CNN models suitable for mobile devices. Arslan [35] combined traditional time-frequency features with CNN-extracted representations through recursive feature elimination and ensemble-based decision making, yielding architectures appropriate for embedded systems.

The methodological diversity has also extended to broader cardiac conditions. Li et al. [36] integrated multi-domain hand-crafted features with CNN-derived MFCC embeddings in a hybrid fusion strategy for coronary artery disease detection. Iqtidar et al. [37] used adaptive local ternary pattern descriptors concatenated with MFCCs after empirical mode decomposition denoising, applying these representations in a machine learning classifier. In the paediatric domain, Oliveira et al. [38] released the CirCor dataset, offering multi-location recordings with rich murmur annotations and auxiliary descriptors such as timing, shape, and pitch, supporting the development of algorithms robust to diverse recording conditions. These advances collectively reflect a shift from isolated algorithmic benchmarks toward integrated, clinically informed systems capable of supporting real-world cardiac screening.

2.3 Quantum-Inspired Deep Learning

Quantum-inspired deep learning (QiDL) is an emerging paradigm that embeds quantum-mechanical principles into classical neural architectures and optimizers. These principles include superposition, entanglement, and unitary evolution. Distinct from full quantum machine learning, which requires quantum hardware, QiDL operates on conventional CPUs and GPUs by simulating quantum phenomena using complex-valued weights, density-matrix representations, and Hilbert-space feature mappings [39]. Key abstractions in QiDL include superposition analogues, where input vectors are mapped to complex amplitudes. This allows a single neuron to encode an exponential number of states. Entanglement proxies are implemented using product-based layers or graph-coupled gates. These components capture high-order correlations without relying on physical qubits. Finally, a density-matrix formalism replaces conventional activations with positive-semidefinite operators, which naturally quantifies epistemic uncertainty

and aligns QiDL with Bayesian inference. These constructions yield richer representational capacity and improved generalization in data-scarce, high-dimensional regimes such as omics, imaging, and longitudinal clinical records.

Optimization techniques span dequantized linear-algebra speedups (Tang-style algorithms), Ising-type energy minimizers [40], and quantum-walk kernels for graph similarity [41]. QiDL’s probabilistic structure dovetails naturally with Bayesian reasoning. Bayesian hyper-parameter tuning deploys quantum-inspired genetic algorithms (QGA) to prune electroencephalogram (EEG) features before feeding a quantum support vector machine (SVM), yielding 57% cross-subject motor-imagery accuracy with $p < 0.03$ significance while using fewer samples than classical SVM [42]. Density-matrix layers output quantum-entropic uncertainties that are propagated through Bayesian neural networks, improving calibration in low-data drug-efficacy trials [40]. Energy-based priors derived from Ising Hamiltonians act as implicit regularizers, shrinking the effective parameter space and mitigating over-fitting in rare-disease genomics. These formulations enable enhanced modeling of uncertainty, relational structure, and non-local dependencies, offering a principled framework for inference under noise and partial observability.

The use of Hilbert space embeddings allows for high-dimensional feature representations that capture subtle patterns in the data, while complex-valued activations facilitate phase-sensitive interference effects analogous to quantum coherence, enhancing sensitivity to semantic and structural nuances in multimodal biomedical signals. Furthermore, quantum-inspired similarity measures based on fidelity between probabilistic state representations have demonstrated superior performance in capturing global structural relationships [41]. This advantage is especially evident in sequential and graph-structured data. Together, these synergies enhance robustness, interpretability, and sample efficiency, three critical attributes for clinical deployment.

Table 1: Impact of quantum-inspired models in biomedical applications.

Domain	Model	Task	Key Result
Psychiatry	QGA-QSVM [42]	Depression screening from EEG	Statistically superior with 20% less training data
Endocrinology	QuCNet [43]	Thyroid-nodule malignancy	97.6% accuracy on limited ultrasound data
Cardiology	QiEA-SMGLR [44]	Denoising phonocardiograms	100% max SNR improvement, $\rho \approx 0.99$ clinical correlation
Clinical NLP	QPFE-ERNIE [45]	Sentiment & word-sense disambiguation in EHR notes	+8.7 F1 over prior quantum models
Neuro-imaging	IDLQET-BTEDC [46]	Brain-tumor edge detection & classification	98% accuracy, Dice=89%, superior to DeepMedic

As indicated in Table 1, these studies collectively show consistent improvements in accuracy, convergence speed, and noise resilience across modalities where the data are scarce, high-dimensional, or privacy-sensitive. Nevertheless, several challenges remain. These challenges and emerging directions characterize current research in quantum-inspired deep learning:

- **Computational overhead:** Simulating entanglement on classical hardware incurs computational cost. Tensor-network approximations can partially mitigate this bottleneck but do not eliminate it entirely [39].
- **Interpretability:** Complex-valued weights and entanglement proxies pose challenges for human interpretability. Recent studies explore quantum-circuit visualizations and entanglement-entropy heat maps as tools for better model explainability [45].
- **Hardware limitations:** Physical quantum accelerators remain prone to noise and decoherence. Hybrid pipelines have been proposed, in which only the optimization layer is offloaded to near-term quantum processing units (QPUs) while inference remains classical [47].
- **Future directions:** Promising research avenues include pretrained quantum-inspired transformers for multi-modal electronic health record (EHR) fusion, quantum federated learning (QFL) using blind quantum computation and quantum key distribution for privacy-preserving training across hospitals [47], and Bayesian-quantum co-design approaches where hyperpriors are optimized via variational quantum eigensolvers and the model uncertainty is back-propagated through quantum-aware layers.

As QiDL matures, the confluence of Bayesian inference, quantum metaphors, and classical deep learning is poised to deliver robust, sample-efficient solutions for precision medicine and population health analytics. Table 2 summarizes the key quantum-inspired learning paradigms, highlighting their core computational mechanisms, empirical gains

across diverse tasks, and the practical bottlenecks reported in the literature. This integrated overview illustrates how different families of models range from tensor-network approaches to quantum-inspired CNNs, DBNs, GNNs, and pre-trained NLP architectures. These models balance theoretical advantages with implementation constraints. The summary provides a foundation for informed selection and further development of QiDL architectures.

Table 2: Summary of quantum-inspired models: core mechanisms, empirical gains, and practical bottlenecks.

Family	Model	Core Mechanism	Reported Advantage	Acknowledged Disadvantage
Tensor-Network Models	MPS/TTN [39]	Low-rank tensor contractions emulating exponentially large Hilbert spaces	Polynomial runtime for tasks classically NP-hard; exponential parameter compression	Cubic-to-quartic scaling in bond dimension D ; collapses on high-res images or large vocabularies; slower than CNN/Transformer at realistic sizes
Quantum-Inspired CNNs	QuCNet [43]	Random quantum-circuit filters applied to 2×2 convolutional patches	97.6% thyroid-nodule accuracy with 5–30% fewer parameters vs. DenseNet121	8.15 h GPU training; performance degrades with >2 circuit repetitions; exponential cost in kernel size forces tiny 2×2 kernels
Quantum-Inspired GNNs	QiEA-SMGLR [44]	Sorted-mutation evolutionary search over FIR-filter coefficients	20–100% SNR gain in PCG denoising; $\rho \approx 0.99$ clinical fidelity	Per-generation filter evaluation \rightarrow heavy CPU load; tiny 6-clip study; fixed 4-tap filter cannot handle richer spectra without exploding search space
Pre-trained NLP	QPFE-ERNIE [45]	ERNIE embeddings fused with complex-valued GRU “evolution circuits”	+8.7 F1 on sentiment tasks; interpretable quantum phase parameters	Training cost doubles (two forward passes per batch); fragile hand-tuned hyper-parameters; extra pre-training stage required
Quantum-Inspired DBNs	QISOA-DBN [48]	Seagull optimiser with qubit-rotation gates and superposition states	98.6% CVD accuracy; $3 \times$ faster convergence than grid-search baselines	Resource-hungry five-layer DBN prone to over-fitting; doubtful transferability to non-cardiac domains; high energy footprint

Building upon the foundational principles of quantum-inspired deep learning, this study extends recent probabilistic and architectural advances by introducing a framework that embeds structured stochasticity into the learning process. Our approach draws inspiration from unitary transformations and density-based representations to ensure consistency between uncertainty modeling and temporal feature extraction. This integration, detailed in the following section, aims to address persistent challenges in biomedical time-series analysis such as data scarcity, noise sensitivity, and interpretable uncertainty estimation.

3 Datasets

This study employs two publicly available PCG datasets, the PhysioNet/computing in cardiology challenge 2016 dataset (CinC) [49] and the CirCor DigiScope dataset 2022 (CirCor) [50]. Both datasets provide real-world heart sound recordings with clinical annotations, but they differ notably in demographic composition, acquisition protocols, labeling schemes, and structural organization. These differences present complementary challenges for developing and evaluating robust and portable cardiac sound analysis methods.

3.1 PhysioNet/CinC Challenge 2016 Dataset (CinC)

The CinC dataset, introduced as part of the PhysioNet Computing in Cardiology Challenge 2016, aggregates PCG recordings from multiple international sources. The recordings were collected in diverse settings, ranging from controlled clinical environments to unstructured non-clinical contexts, using a variety of digital stethoscopes and mobile devices. Participants’ ages span from 18 to 85 years, with a near-balanced gender distribution. This heterogeneity introduces real-world variability in recording quality and background interference, making the dataset particularly valuable for evaluating model robustness under practical conditions.

The dataset is organized into six labeled subsets, *training-a* through *training-f*, contributed by different institutions. Only *training-a* contains actual PCG recordings; therefore, this subset is used exclusively. This subset contains 409 recordings from unique adult subjects, each annotated as Normal or Abnormal. Variable recording durations and inconsistent signal quality further increase the realism and challenge of the dataset.

Table 3: Summary of the CinC dataset.

Feature	Description
Number of recordings	409 (training-a subset)
Number of subjects	409
Classes	Normal / Abnormal
Age group	18–85 years
Recording environment	Clinical / Non-clinical
Noise contamination	Moderate

3.2 CirCor DigiScope Dataset 2022 (CirCor)

The CirCor dataset, released for the George B. Moody PhysioNet Challenge 2022, represents one of the largest publicly available pediatric PCG collections. It includes 3,136 recordings from 942 subjects, gathered during two mass screening campaigns in northeastern Brazil, CC2014 and CC2015. Unlike CinC, which focuses on adults, CirCor is predominantly pediatric, with children constituting over 70% of the cohort, complemented by infants, adolescents, and a small number of neonates.

Recordings were captured from up to five auscultation sites per subject, with the majority originating from the four canonical valve positions: aortic (AV), pulmonary (PV), tricuspid (TV), and mitral (MV). This multi-site structure enables spatial analysis of murmurs but introduces inter-recording variability for the same subject. The dataset provides two complementary annotation layers: (1) murmur status, categorized as Absent, Present, or Unknown, and (2) clinical outcome, labeled as Normal or Abnormal. For binary classification, this study uses only the Absent and Present murmur labels. CirCor presents several challenges inherent to real-world screening. Recordings contain pervasive environmental noise, including stethoscope handling artifacts, ambient speech, crying, and traffic sounds, some of which spectrally overlap with diagnostically relevant heart sounds. Additionally, the distribution of murmur labels is imbalanced, with significantly more Absent than Present cases, posing a challenge for supervised learning without careful handling of class representation.

Table 4: Summary of the CirCor dataset.

Feature	Description
Number of subjects	942
Number of recordings	3,136
Classes (murmur)	Absent / Present (Unknown excluded)
Age group	Primarily children
Auscultation locations	AV, PV, TV, MV
Noise contamination	Moderate to high, real-world conditions

While both datasets used in this study support binary heart sound classification, they differ fundamentally in scope and structure. The CinC dataset emphasizes adult cardiac assessment across heterogeneous acquisition conditions, with one recording per subject and a focus on global abnormality detection. In contrast, CirCor provides a pediatric-focused, multi-site recording structure with fine-grained murmur annotations and greater temporal and spatial variability.

4 Methodology

4.1 Variational Convolution with Quantum-Inspired Sampling

This research introduces QiVConv, a probabilistic convolutional layer that enhances uncertainty modeling through a novel sampling method. A demonstration implementation of the proposed methodology is publicly available on GitHub. The repository includes the QiVConv layer and the RFR block, <https://github.com/amingolnari/Demo-QiVC-Net>.

Unlike standard variational layers that perturb kernel weights using unstructured Gaussian noise, QiVConv leverages structured stochasticity derived from principles of quantum state evolution. Specifically, a unitary-rotated variational sampling mechanism is introduced, in which structured uncertainty is injected via rotated variational sampling with subspace swapping, while preserving full differentiability and enabling more expressive posteriors.

The multichannel one-dimensional input signal is denoted by $\mathbf{X} \in \mathbb{R}^{T \times C_{in}}$, where T represents the number of time steps and C_{in} the number of input channels. The convolutional kernel $\mathbf{W} \in \mathbb{R}^{K \times C_{in} \times C_{out}}$, where K is the kernel size

and C_{out} the number of filters, is modeled as a Gaussian-distributed parameter $\mathbf{W} \sim \mathcal{N}(\boldsymbol{\mu}, \boldsymbol{\sigma}^2)$, and samples during training are drawn using the re-parameterization trick proposed by Kingma & Welling [51].

$$\mathbf{W} = \boldsymbol{\mu} + \boldsymbol{\sigma} \odot \boldsymbol{\epsilon}_{\text{init}} \quad (1)$$

Here, $\boldsymbol{\mu}$ and $\boldsymbol{\sigma}$ represent the mean and standard deviation. The initial noise $\boldsymbol{\epsilon}_{\text{init}}$ is sampled from a Gaussian distribution. In the subsequent processing stage, this noise is transformed via QR decompositions, unitary rotations, and controlled depolarizing noise so that the resulting non-Gaussian perturbation $\boldsymbol{\epsilon}_{\text{QIRE}}$ replaces the conventional re-parameterization term $\boldsymbol{\sigma} \odot \boldsymbol{\epsilon}_{\text{init}}$.

4.1.1 Quantum-Inspired Unitary-Rotated Variational Sampling

Traditional variational inference typically injects randomness into the model weights using unstructured Gaussian noise. However, this approach can produce noise that is misaligned with the intrinsic geometry of the parameter space, potentially causing unstable training dynamics or poor calibration. To overcome this limitation, our method draws inspiration from the mathematical framework of quantum mechanics. Reliability-focused approaches have demonstrated that mathematically constrained, norm-preserving transformations within parameter spaces improve robustness to uncertainty [52]. These insights align closely with the objectives of our QiVConv framework, which utilizes rotated variational sampling with subspace swap to inject structured stochasticity while maintaining geometric coherence.

4.1.2 Inter-Channel Correlation and Kernel Vectorization

A critical feature of the QiVConv mechanism is its holistic treatment of the kernel weights. The convolutional kernel \mathbf{W} is first vectorized into a single vector $\mathbf{w} \in \mathbb{R}^N$, where $N = K \cdot C_{\text{in}} \cdot C_{\text{out}}$. By rotating the entire kernel vector \mathbf{w} within its subspace, structured stochasticity is introduced across every component, including spatial and inter-channel correlations. This approach avoids the need for an explicit layer to model channel correlation, achieving an efficient coupled uncertainty injection over the entire parameter space.

In quantum theory, pure states are represented as unit vectors on a hypersphere within a complex Hilbert space, and their evolution is governed by unitary operations that rotate these vectors without altering their norm or internal structure [6]. This concept of geometry-preserving stochastic evolution offers a compelling analogy for constructing noise processes in neural networks. Accordingly, our approach treats the vectorized noise similarly to a quantum state: rather than injecting noise randomly, it undergoes a structured rotation within a low-dimensional subspace of the weight space, preserving both its norm and coherence.

The procedure to generate such noise is as follows:

1. **Flattening:** Reshape the kernel weight \mathbf{W} (the noise $\boldsymbol{\epsilon}_{\text{init}}$) into a vector $\mathbf{w} \in \mathbb{R}^N$.
2. **Random subspace generation:** Draw a random matrix $\mathbf{G} \in \mathbb{R}^{N \times k}$ with entries sampled from $\mathcal{N}(0, 1)$, and compute its QR decomposition to obtain an orthonormal basis:

$$\mathbf{G} = \mathbf{Q}\mathbf{R}, \quad \mathbf{Q} \in \mathbb{R}^{N \times k}. \quad (2)$$

The columns of \mathbf{Q} span a k -dimensional subspace of \mathbb{R}^N .

3. **Amplitude encoding:** Sample a base noise vector $\boldsymbol{\epsilon}_0 \sim \mathcal{N}(0, \mathbf{I}_N)$ and normalize it:

$$\boldsymbol{\epsilon} \leftarrow \frac{\boldsymbol{\epsilon}_0}{\|\boldsymbol{\epsilon}_0\|}, \quad (3)$$

projecting it onto the unit hypersphere, analogous to encoding a normalized quantum state.

4. **Unitary rotation:** Sample a rotation matrix $\mathbf{U} \sim \text{Haar}(\text{SO}(k))$ and perform a structured rotation in the subspace defined by \mathbf{Q} :

$$\boldsymbol{\epsilon}_{\text{rot}} = \mathbf{Q}\mathbf{U}\mathbf{Q}^T \boldsymbol{\epsilon}. \quad (4)$$

This rotation whitens the noise and introduces structured stochasticity while preserving the norm and subspace structure.

5. **Variational update (subspace swap):** Construct the final noise vector by swapping the component of the initial noise that lies within the subspace \mathbf{Q} with the newly rotated component $\boldsymbol{\epsilon}_{\text{rot}}$, while keeping the orthogonal component unchanged:

$$\epsilon_{\text{final}} \leftarrow \epsilon - \mathbf{Q}\mathbf{Q}^\top \epsilon + \epsilon_{\text{rot}}. \quad (5)$$

This operation ensures that the noise remains aligned with the rotational subspace while preserving the overall variance of the original noise.

6. **Optional decoherence:** Optionally apply depolarizing noise to simulate decoherence effects:

$$\epsilon_{\text{final}} \leftarrow \mathbf{m} \odot \epsilon_{\text{final}} + (1 - \mathbf{m}) \cdot \frac{\mathbf{1}}{\sqrt{N}}, \quad \mathbf{m} \sim \text{Bernoulli}(1 - p), \quad (6)$$

where p controls the noise level and $\mathbf{1}$ is the unit vector.

The resulting noise vector ϵ_{final} is reshaped to match the dimensions of \mathbf{W} and applied in the variational convolution. The final weights then compute as $\mathbf{W} = \boldsymbol{\mu} + \boldsymbol{\sigma} \odot \epsilon_{\text{final}}$. It was experimentally observed that setting the subspace dimensionality k between 2 and 9 provides computational efficiency while maintaining performance. In the experiments conducted, the value of k is set to 5. This unitary-rotated variational sampling introduces coherent geometric structures into the variational space, leading to smoother uncertainty propagation, enhanced regularization, and more calibrated predictive distributions. The overall procedure is summarized in Algorithm 1.

4.1.3 Variational Inference and Regularization

The total objective of the QiVConv layer is defined by minimizing the evidence lower bound (ELBO), as the result of combining the task-specific loss with a KL divergence term that regularizes the weight distributions. The variational posterior is parameterized by a mean $\boldsymbol{\mu}$ and a standard deviation $\boldsymbol{\sigma}$. The standard deviation is derived from a learnable parameter $\boldsymbol{\rho}$ via the softplus function to enforce non-negativity:

$$\boldsymbol{\sigma} = \text{softplus}(\boldsymbol{\rho}) = \log(1 + e^\rho).$$

During inference (test time), the deterministic output $\hat{\mathbf{Z}}$ is computed by using the posterior mean of the variational kernel, which is defined as:

$$\hat{\mathbf{Z}} = \phi(\mathcal{C}(\mathbf{X}; \boldsymbol{\mu}) + \mathbf{b}), \quad (7)$$

where $\mathcal{C}(\cdot)$ denotes the convolution operator, \mathbf{b} is the bias term, and ϕ is a non-linear activation function. To regularize the variational distribution, the Kullback–Leibler (KL) divergence between the learned posterior distribution $q(\mathbf{W}|\boldsymbol{\mu}, \boldsymbol{\sigma})$ and the prior distribution $p(\mathbf{W}|\sigma_{\text{prior}})$ is minimized:

$$\text{KL}(q\|p) = \sum \left[\frac{\boldsymbol{\sigma}^2 + \boldsymbol{\mu}^2}{2\sigma_{\text{prior}}^2} - \log(\boldsymbol{\sigma} + \varepsilon) + \log \sigma_{\text{prior}} - \frac{1}{2} \right], \quad (8)$$

The sum is computed over all weights and biases in the convolutional layer, and the small constant ε ensures numerical stability. The total objective function minimized during training is the following:

$$\mathcal{L}_{\text{Total}} = \mathcal{L}_{\text{Task}}(\mathbf{Z}, \mathbf{Y}) + \lambda \cdot \text{KL}(q\|p), \quad (9)$$

where $\mathcal{L}_{\text{Task}}$ is the data likelihood loss and λ is a weight factor controlling the strength of the KL regularization.

4.2 Pre-processing

The preprocessing pipeline was designed to enhance the quality and consistency of PCG recordings while preserving diagnostically relevant acoustic features. All recordings were band-pass filtered between 25 Hz and 400 Hz using a fourth-order zero-phase Butterworth filter, consistent with established PCG signal processing practices reported in previous studies [20]. This frequency range captures the main components of S_1 and S_2 heart sounds and most pathological murmurs, while attenuating respiratory noise and high-frequency artifacts.

Each recording was then segmented into consecutive, non-overlapping windows of fixed 4 s duration. This approach ensures complete temporal coverage and uniform segment length suitable for batch processing. Each segment contains multiple cardiac cycles across typical heart rates (60 to 150 bpm), allowing the model to capture continuous acoustic dynamics, including murmurs, pauses, and inter-cycle variability, without assuming regular cardiac periodicity.

Algorithm 1 QiVC layer: quantum-inspired variational convolution

Require: Kernel \mathbf{W} (random), subspace dim. $k = 5$, decoherence $p = 0.05$, prior var. $\sigma_{\text{prior}}^2 = 0.01$, KL scale $\lambda = 1 \times 10^{-5}$, noise ϵ_0

Ensure: Noisy kernel $\mathbf{W}_{\text{noisy}}$, KL loss

```

1: function ORTHONORMALBASIS( $N, k$ )
2:    $\mathbf{G} \sim \mathcal{N}(0, 1)^{N \times k}$            ▷ Generate random Gaussian matrix of size  $N \times k$ 
3:    $[\mathbf{Q}, \mathbf{R}] \leftarrow \text{QR}(\mathbf{G})$      ▷ Compute QR decomposition for orthonormal basis
4:   return  $\mathbf{Q}$                          ▷ Return orthonormal basis of the subspace
5: end function
6: function HAARSO( $k$ )
7:    $\mathbf{A} \sim \mathcal{N}(0, 1)^{k \times k}$          ▷ Random Gaussian matrix for generating Haar unitary
8:    $[\mathbf{Q}, \mathbf{R}] \leftarrow \text{QR}(\mathbf{A})$      ▷ Compute QR decomposition to orthogonalize
9:    $\mathbf{D} \leftarrow \text{diag}(\text{sign}(\text{diag}(\mathbf{R})))$  ▷ Correct signs for a proper orthogonal matrix
10:   $\mathbf{U} \leftarrow \mathbf{Q}\mathbf{D}$                 ▷ Unitary matrix sampled from Haar measure
11:  if  $\det(\mathbf{U}) < 0$  then
12:     $\mathbf{U}_{:,1} \leftarrow -\mathbf{U}_{:,1}$      ▷ Ensure special orthogonal matrix ( $\det=+1$ )
13:  end if
14:  return  $\mathbf{U}$                            ▷ Return rotation matrix
15: end function
16: function QIVCSAMPLE( $\mathbf{W}, k, p$ )
17:   $\mathbf{w} \leftarrow \text{vec}(\mathbf{W})$                  ▷ Flatten kernel to vector
18:   $N \leftarrow |\mathbf{w}|$                      ▷ Compute Number of elements in kernel
19:   $\epsilon \sim \mathcal{N}(0, \mathbf{I}_N)$                  ▷ Sample isotropic Gaussian noise
20:   $\epsilon \leftarrow \epsilon_0 / \|\epsilon_0\|_2$        ▷ Normalize noise vector (amplitude encoding)
21:   $\mathbf{Q} \leftarrow \text{ORTONORMALBASIS}(N, k)$  ▷ Sample random subspace of dimension  $k$ 
22:   $\mathbf{U} \leftarrow \text{HAARSO}(k)$            ▷ Sample random unitary rotation in subspace
23:   $\epsilon_{\text{rot}} \leftarrow \mathbf{Q}\mathbf{U}\mathbf{Q}^T \epsilon$    ▷ Rotate noise in low-dimensional subspace
24:   $\epsilon_{\text{final}} \leftarrow \epsilon - \mathbf{Q}\mathbf{Q}^T \epsilon + \epsilon_{\text{rot}}$  ▷ Combine rotated and orthogonal noise components
25:  if  $p > 0$  then
26:     $\mathbf{m} \sim \text{Bernoulli}(1 - p)^N$        ▷ Sample decoherence mask (drop probability  $p$ )
27:     $\epsilon_{\text{final}} \leftarrow \mathbf{m} \odot \epsilon_{\text{final}} + (1 - \mathbf{m}) / \sqrt{N}$  ▷ Apply decoherence to noise
28:  end if
29:  return  $\text{reshape}(\epsilon_{\text{final}}, \text{shape}(\mathbf{W}))$  ▷ Reshape noise to original kernel shape
30: end function
31: procedure QIVCLAYER( $\mathbf{X}, \mu, \rho, \mathbf{b}, k, p, \lambda, \sigma_{\text{prior}}$ )
32:   $\sigma \leftarrow \text{softplus}(\rho)$            ▷ Compute standard deviation via softplus to ensure positivity
33:   $\mathbf{W}_s \leftarrow \mu + \sigma \odot \text{QIVCSAMPLE}(\mu, k, p)$  ▷ Sample noisy kernel using reparameterization trick
34:   $\mathbf{Z} \leftarrow \phi(\mathcal{C}(\mathbf{X}; \mathbf{W}_s) + \mathbf{b})$    ▷ Forward pass: convolution + bias + activation
35:   $\mathcal{L} \leftarrow \text{TaskLoss}(\mathbf{Z}, \mathbf{Y}) + \lambda \sum \left[ \frac{\sigma^2 + \mu^2}{2\sigma_{\text{prior}}^2} - \log \sigma + \log \sigma_{\text{prior}} - \frac{1}{2} \right]$  ▷ Total loss = task loss + KL divergence
36:  return  $\mathcal{L}, \mathbf{Z}$                        ▷ Return loss and layer output
37: end procedure

```

Finally, each segment was resampled to 2000 samples (effective 500 Hz), mean-centered to remove baseline drift, and amplitude-normalized to the range ± 1.0 . Segments containing non-finite or zero-valued samples were discarded to maintain numerical stability during training. Figures 1 and 2 present representative PCG signal samples from the CinC and CirCor datasets, respectively, illustrating the distinct characteristics and variability of heart sounds across both sources.

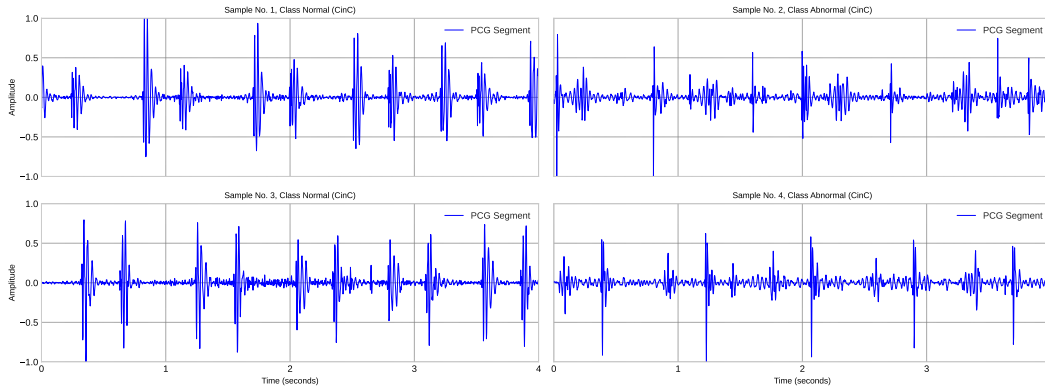


Figure 1: Representative PCG signal segments from the CinC dataset, depicting normal and with murmur heart sounds across different recording conditions.

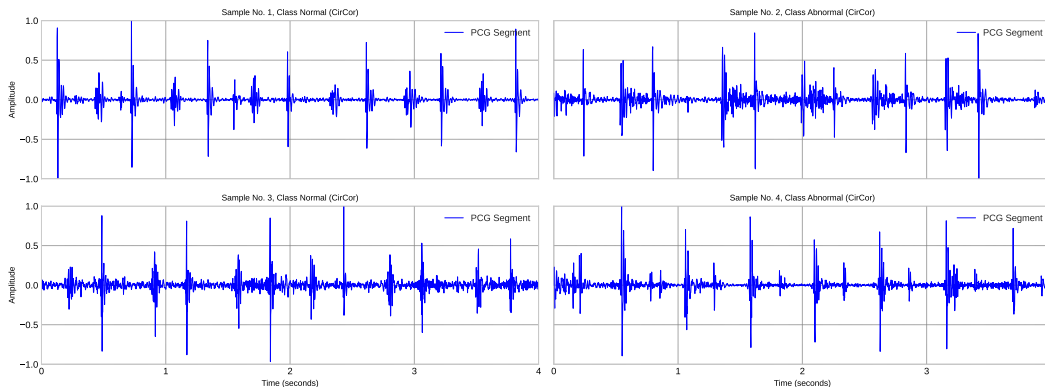


Figure 2: Representative PCG signal segments from the CirCor dataset, depicting normal and with murmur heart sounds across different recording conditions.

4.3 Evaluation Metrics

To evaluate classification models, several key metrics are used to assess accuracy, robustness, and clinical reliability. These are derived from the confusion matrix, which defines true positives (TP), false positives (FP), true negatives (TN), and false negatives (FN), with abnormal heart sounds treated as positive and normal sounds as negative. Accuracy measures the overall proportion of correct predictions. Sensitivity (recall) evaluates the model’s ability to detect abnormal cases, which is critical in medical diagnosis. Specificity measures correct identification of normal cases, reducing false alarms. The F1 score provides a unified measure of model performance by harmonizing true positive rate and positive predictive value, making it particularly valuable in scenarios where class distributions are skewed. Together, these metrics provide a comprehensive evaluation of a model’s performance in clinical and real-world settings.

The mathematical formulations of these evaluation metrics are as follows. Accuracy is defined as the ratio of correctly predicted instances to the total number of instances:

$$\text{Accuracy} = \frac{TP + TN}{TP + TN + FP + FN} \quad (10)$$

$$\text{Sensitivity} = \frac{TP}{TP + FN} \quad (11)$$

$$\text{Specificity} = \frac{TN}{TN + FP} \quad (12)$$

$$F1\text{-score} = \frac{2 \cdot TP}{2 \cdot TP + FP + FN} \tag{13}$$

These formulas collectively support a rigorous and clinically meaningful evaluation of PCG classification approaches, enabling reliable comparison across different models and datasets.

4.4 Proposed Architecture

In this research, a novel deep learning architecture for PCG classification is proposed, integrating temporal symmetry modeling, uncertainty-aware representation learning, and hierarchical feature extraction. The model is built upon the RFR block, a custom residual unit designed to capture bidirectional physiological dynamics in heart sound sequences. Each RFR block processes the input through a dual-path scheme consisting of a forward path and a time-reversed backward path, both operating on the same segment. The outputs of these paths are then fused using long short-term memory (LSTM) layers and residual connections, enabling the model to capture both local and long-range temporal dependencies. Instead of employing a simple addition for the residual connection, the shortcut is concatenated with the fused features and the result is refined using an LSTM layer. The RFR block consists of three main components:

1. **Shortcut path:** A 1×1 convolution followed by batch normalization and a non-linear activation provides a residual connection, refine channel dimension without learning entirely new representations.
2. **Forward and backward paths:** The forward path applies a QiVConv layer followed by batch normalization and activation. The backward path processes a time-reversed version of the input through an identical QiVConv layer and then reverses the output back to the original temporal order. This design captures complementary forward and reverse temporal features.
3. **Fusion and refinement:** The outputs of the forward and backward paths are concatenated and fused using a LSTM layer. Batch normalization and activation follow to produce a refined representation. Finally, the fused features are concatenated with the shortcut path and further processed by another LSTM, batch normalization, and activation to produce the final block output.

Multiple RFR blocks are stacked with progressively increasing filter counts and interspersed downsampling, enabling hierarchical abstraction of PCG features. Global max pooling is applied before the output layer to ensure invariance to sequence shifts. Finally, a fully connected layer followed by a softmax classifier produces a binary decision between normal and abnormal classes. The RFR block architecture is illustrated in Figure 3.

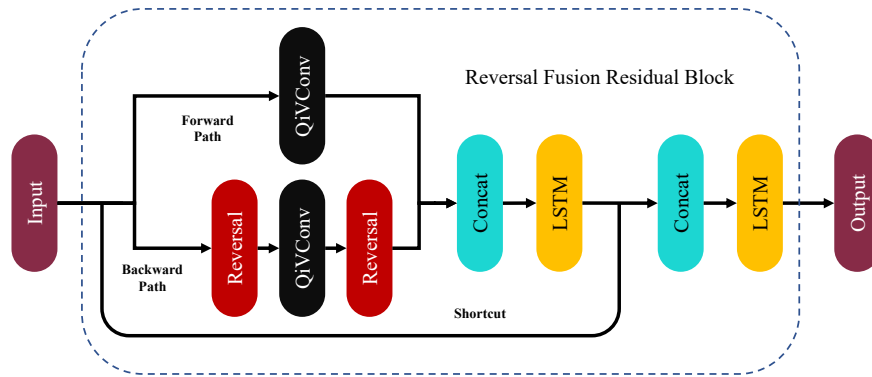


Figure 3: Reversal fusion residual block architecture.

4.5 Training Strategy

As shown in Figure 4, there is a significant class imbalance in both the CinC and CirCor datasets, with a larger proportion of normal heart sound recordings compared to abnormal ones. To effectively address this issue, the proposed QiVC-Net is trained using a composite loss function that combines categorical cross-entropy (CCE) denoted as \mathcal{L}_{CCE} and Dice loss denoted as \mathcal{L}_{Dice} , balancing sample-wise classification accuracy with region-level overlap. A dynamic loss weighting mechanism, inspired by our previous work [53], adaptively penalizes and reweights each loss component in real time during training, allowing the model to emphasize the most informative objective at different stages. This

adaptive strategy improves convergence and generalization under noisy and data-imbalanced conditions. Additionally, to prevent overfitting, early stopping was applied alongside model checkpointing to retain the best-performing weights based on validation performance throughout training.

$$\mathcal{L}_{\text{CCE}} = -\frac{1}{N} \sum_{i=1}^N \sum_{c=1}^C y_{i,c} \log(\hat{y}_{i,c}) \quad (14)$$

$$\mathcal{L}_{\text{Dice}} = 1 - \frac{2 \sum_{i=1}^N y_i \hat{y}_i}{\sum_{i=1}^N y_i + \sum_{i=1}^N \hat{y}_i} \quad (15)$$

The training process was conducted for over 500 epochs per experiment, with a batch size of 256 and a learning rate of 1×10^{-3} , using stratified 5-fold cross-validation to ensure balanced representation of both classes in each fold. Additionally, to prevent overfitting, early stopping was employed alongside model checkpointing, ensuring that the training process is terminated once the performance on the validation set ceased to improve. In this strategy, the model continuously monitors the performance at each epoch and stores the weights corresponding to the best observed validation metric. This approach ensures that, even if overfitting occurs in later epochs, the model retains the set of weights that achieved the best generalization performance on the validation set for final evaluation and inference [54]. Experimental observations revealed that the optimal validation performance does not always coincide with the minimum training loss, as excessive loss minimization may lead to overfitting or reduced generalization capability.

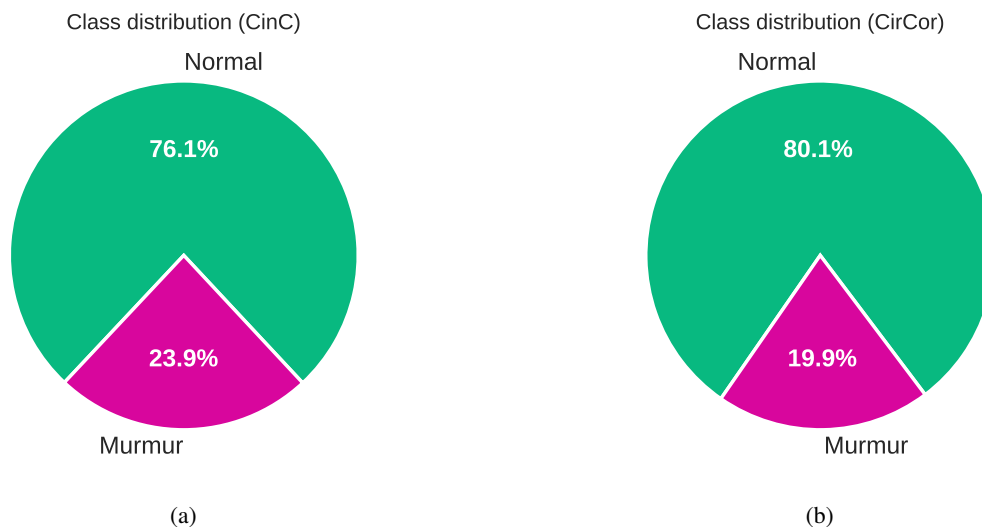


Figure 4: Class distribution in the PCG datasets: (a) CinC and (b) CirCor.

5 Results

This section presents the experimental evaluation of the proposed QiVC-Net on two benchmark datasets for PCG classification. To ensure robustness and statistical reliability, we performed 5-fold stratified cross-validation on both datasets and report key performance metrics including accuracy, sensitivity, specificity, and F1-score. The following results highlight the model’s ability to distinguish between normal and abnormal cardiac auscultations under real-world conditions characterized by noise, signal variability, and significant class imbalance.

Table 5 presents the 5-fold stratified cross-validation results of the proposed QiVC-Net on the CinC and CirCor datasets. As shown in the table, the model achieves strong and consistent performance across both datasets. On the CinC dataset, it records an average accuracy of 97.84%, with specificity, sensitivity, and F1-score of 98.14%, 96.89%, and 97.41%, respectively, demonstrating balanced classification capability. Similarly, on the CirCor dataset, the model attains an average accuracy of 97.89%, a high specificity of 99.27%, a sensitivity of 92.34%, and an F1-score of 95.71%. These results highlight the model’s strong generalization across folds, reliable detection of both normal and abnormal heart sounds, and robustness to class imbalance.

Table 5: 5-Fold stratified cross-validation results on CinC and CirCor datasets.

Dataset	Fold	Accuracy (%)	Specificity (%)	Sensitivity (%)	F1-score (%)
CinC	Fold 1	98.44	98.59	97.98	96.73
	Fold 2	96.57	96.13	97.89	93.45
	Fold 3	98.87	99.04	98.28	97.56
	Fold 4	97.99	99.41	93.66	95.82
	Fold 5	97.31	97.51	96.65	94.43
	Average	97.84	98.14	96.89	95.60
CirCor	Fold 1	98.64	99.54	94.98	96.50
	Fold 2	98.28	99.61	93.28	95.79
	Fold 3	98.14	99.48	92.52	95.03
	Fold 4	95.96	98.14	87.11	89.48
	Fold 5	98.42	99.58	93.78	95.95
	Average	97.89	99.27	92.34	95.55

Table 6: Benchmarking of various deep learning-based PCG classification methods on the CirC and CirCor datasets. “N/A” indicates that the corresponding metric was not reported in the original study.

Dataset	Paper	Methodology	Accuracy (%)	Sensitivity (%)	Specificity (%)	F1-score (%)	
CirC	[55]	Recognizing recurrent neural network (RRNN)	95.20	91.60	99.10	N/A	
	[56]	1D-CNN, wavelet stockwell transform (WST)	96.51	96.60	96.60	96.42	
	[57]	Hidden semi-Markov model (HSMM), CNN	86.80	87.00	86.60	N/A	
	[58]	Support vector machine (SVM)	91.36	80.28	94.47	N/A	
	[59]	CNN-LSTM	86.00	87.00	89.00	91.00	
	[60]	Ensemble classifier (SVM, KNN, DT, ANN, LSTM)	91.23	78.81	97.04	N/A	
	[61]	Feed-forward neural network (FNN)	85.65	86.73	84.75	84.58	
	[62]	Stacked autoencoder deep neural network (SAE-DNN)	95.43	97.92	98.32	95.75	
	[63]	1D U-Net-based	92.80	94.50	N/A	N/A	
	[64]	Zero-order autonomous learning multiple-model (ALMMo-0)	93.04	90.82	95.26	N/A	
		Ours	QiVC-Net	97.84	96.89	98.14	95.60
	CirCor	[65]	SVM	82.00	N/A	N/A	N/A
		[66]	Stockwell transform, AlexNet deep features, random forest (RF)	92.10	91.00	91.00	N/A
		[67]	SVM	76.61	82.12	54.03	N/A
[68]		Parallel-attentive transformer	79.80	N/A	N/A	65.10	
[69]		ResNet-101	86.00	86.00	N/A	86.00	
[70]		MFCC, KNN	76.31	N/A	N/A	N/A	
[63]		1D U-Net-based	90.30	96.20	N/A	N/A	
[56]		1D-CNN, Wavelet stockwell transform (WST)	90.09	90.14	90.14	90.09	
		Ours	QiVC-Net	97.89	92.34	99.27	95.55

Table 6 summarizes the results of key PCG classification methods, including CNN-, RNN-, Transformer-based, and hybrid models. As shown in Table 6, while many previous methods achieve high specificity, sensitivity is often lower due to class imbalance and noisy signals. In contrast, the proposed QiVC-Net demonstrates consistently strong and balanced performance across both datasets. On the CinC dataset, QiVC-Net achieves an average accuracy of 97.84%, specificity of 98.14%, sensitivity of 96.89%, and F1-score of 95.60%, whereas on the CirCor dataset it reaches an average accuracy of 97.89%, specificity of 99.27%, sensitivity of 92.34%, and F1-score of 95.55%. These results highlight that QiVC-Net not only maintains high overall classification performance but also effectively handles both normal and abnormal heart sounds, demonstrating robustness and stability across folds and datasets in the presence of noise and class imbalance.

Figures 5 and 6 illustrate the robustness of the proposed QiVC-Net against additive noise on the CinC and CirCor datasets, respectively. As shown in the figures across both datasets, the model maintains high classification performance at elevated SNR levels, achieving near-optimal AUC and accuracy, and exhibits a smooth, gradual degradation as noise intensity increases. On the CinC dataset, for example, the model achieves an average AUC around 0.99 and accuracy above 0.97 at 25 dB SNR, while at 10 dB and 5 dB SNRs, accuracy gracefully declines to approximately 0.80 and 0.76. Similarly, on the CirCor dataset, the model retains accuracies above 0.96 at high SNRs and maintains competitive

performance around 0.85 and 0.82 at lower SNRs, with AUC showing a controlled decrease under severe noise. This consistent behavior across datasets indicates that QiVC-Net preserves discriminative capability and confidence calibration even in noisy and challenging recording conditions. The results highlight the robustness and generalization of the variational, uncertainty-aware architecture, demonstrating its suitability for real-world PCG analysis where signal noise is inevitable.

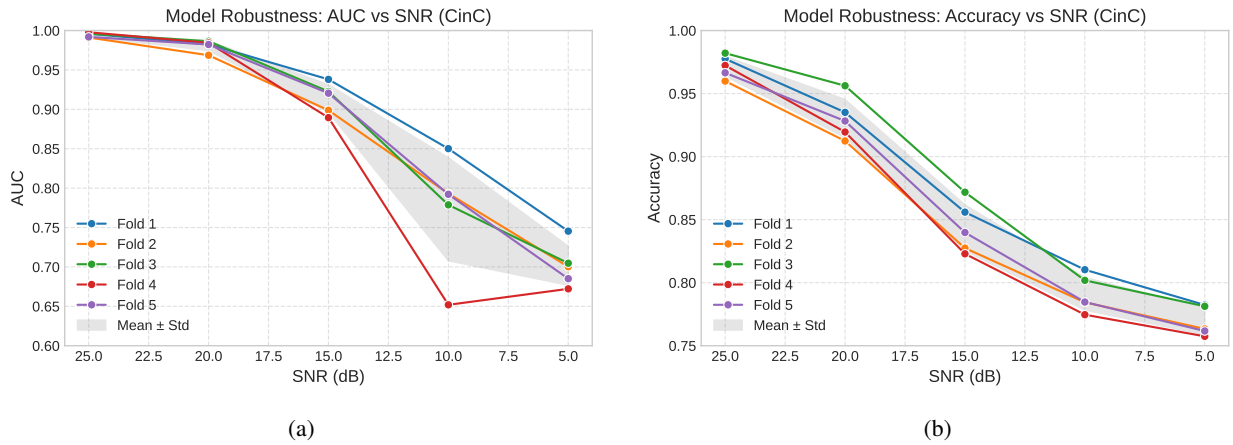


Figure 5: Model robustness on the CinC dataset under varying SNR ratios; (a) AUC vs. SNR, and (b) Accuracy vs. SNR.

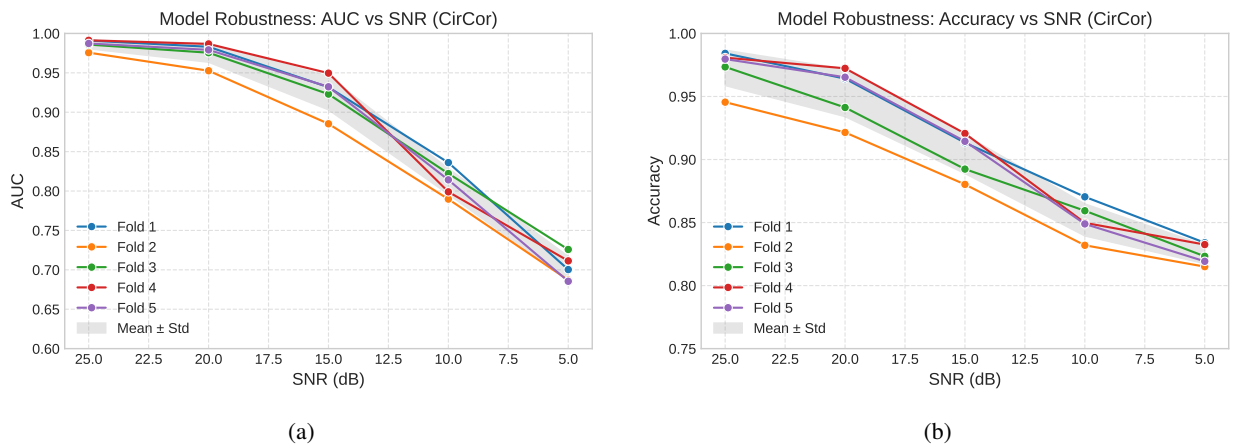


Figure 6: Model robustness on the CirCor dataset under varying SNR ratios; (a) AUC vs. SNR, and (b) Accuracy vs. SNR.

The reliability diagrams in Figure 7 show that the model achieves high accuracy on both datasets while maintaining moderate, uncertainty-aware confidence. Low expected calibration error (ECE) values indicate well-calibrated predictions, aligning confidence with empirical accuracy. This conservative approach is particularly beneficial for noisy and imbalanced biomedical data like PCGs, ensuring reliable predictions without overconfidence on ambiguous signals.

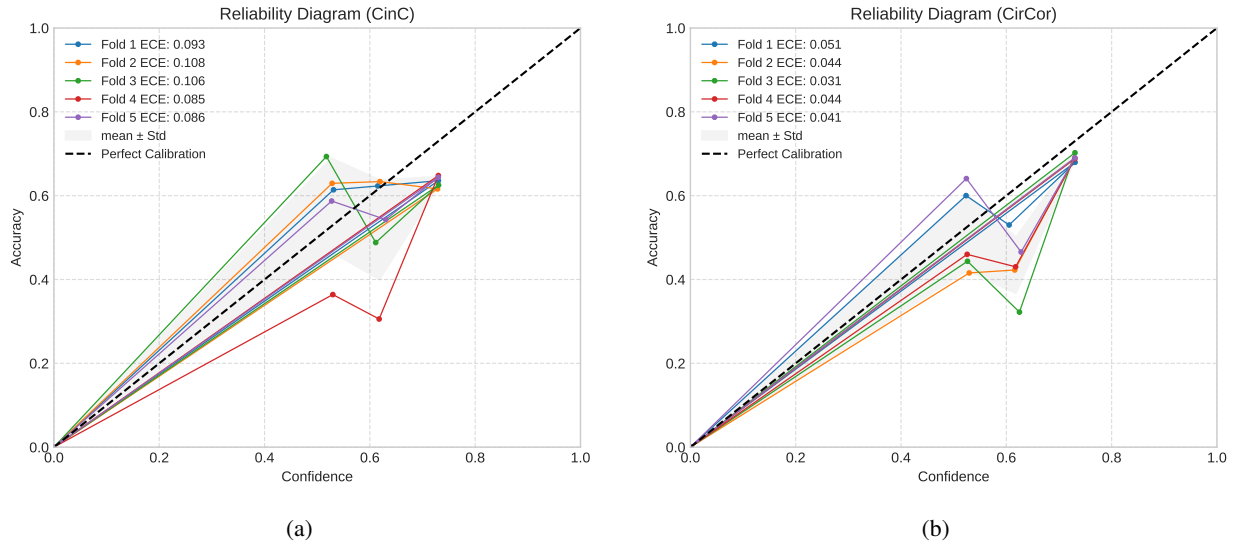


Figure 7: Reliability diagrams comparing model calibration on the CinC and CirCor datasets; (a) Calibration curve for the CinC dataset and (b) calibration curve for the CirCor dataset. The x-axis represents predicted confidence (mean predicted probability per bin) and the y-axis shows observed accuracy (fraction of positive cases) within each bin. The dashed diagonal line indicates perfect calibration.

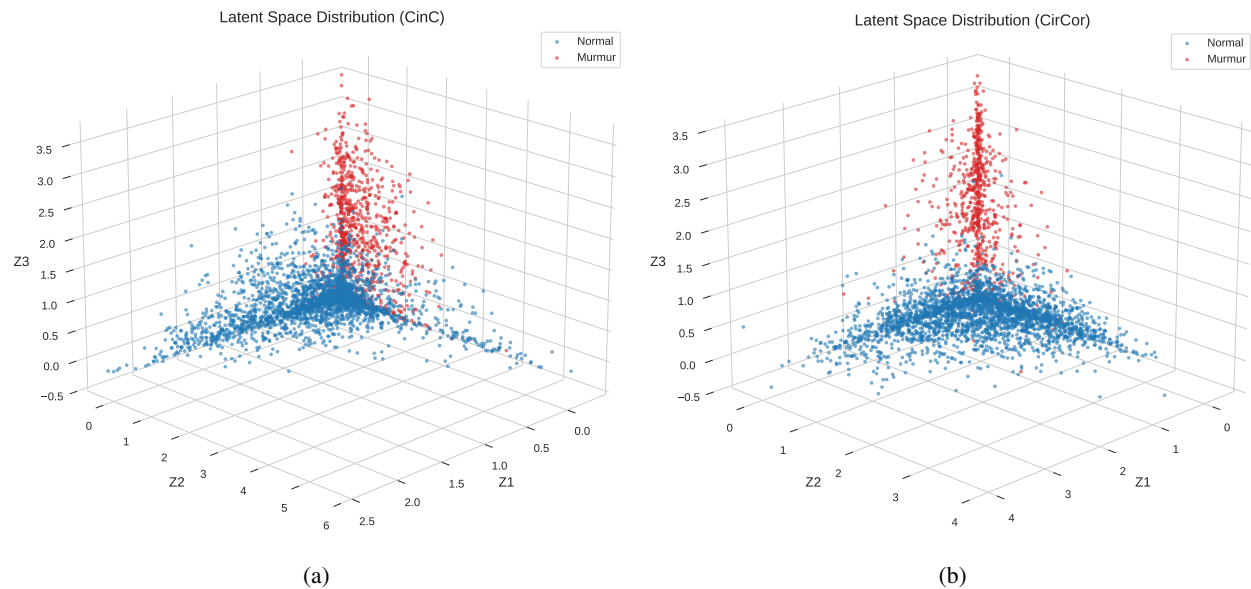


Figure 8: 3D latent space distribution of the model’s bottleneck features for (a) CinC and (b) CirCor datasets.

To better interpret the learned representations, the latent space of the model’s bottleneck is visualized by selecting one model from the 5-fold cross-validation for each dataset. Figure 8 shows a 3D projection of the bottleneck activations onto the first three latent dimensions (Z_1, Z_2, Z_3), with the CinC dataset on the left and the CirCor dataset on the right. The scatter plots reveal distinct clustering patterns for normal and abnormal heart sound recordings, indicating that the model effectively captures discriminative features in its latent space. Points that lie close together represent samples with similar learned representations, while separable clusters demonstrate that the network has learned meaningful class-specific features despite noise and class imbalance.

6 Conclusion

In this study, QiVC-Net, a quantum-inspired variational convolutional network, was proposed for the classification of PCG signals. The model demonstrated consistently high performance across both the CinC and CirCor datasets, achieving average accuracies close to 98%, strong specificity, and competitive sensitivity, while effectively handling class imbalance. Robustness analysis under varying noise conditions indicated that discriminative capability and confidence calibration were maintained even with degraded input signals. Reliability diagrams confirmed that the model produced well-calibrated predictions, reflecting a conservative and uncertainty-aware behavior. Using a composite loss function with dynamic weighting, along with early stopping and stratified cross-validation, the model achieved stable and generalizable performance across folds. Comparative analysis with state-of-the-art methods, such as those in previous studies [56, 62, 64], shows that QiVC-Net outperforms existing approaches while maintaining balanced sensitivity and specificity. Overall, these results demonstrate that variational, uncertainty-aware convolutional architectures are effective for robust classification in challenging, noisy, and corrupted biomedical datasets, including PCG signals. The model maintained reliable performance even under conditions of data imbalance and signal degradation.

The QiVC framework offers several notable advantages. By introducing structured uncertainty modeling through the QiRE mechanism, QiVC enables the model to capture meaningful variability in the convolutional weights while maintaining stable training dynamics. The design remains parameter-efficient, as it does not add additional learnable weights beyond the mean and standard deviation, making the approach suitable for lightweight deployment. Moreover, QiVC leads to improved prediction calibration and helps prevent over-confidence, particularly in noisy or ambiguous cases, an important factor in clinical and safety-critical applications. While QiVC demonstrates clear benefits in uncertainty modeling and calibration, some aspects remain open for refinement. The quantum-inspired rotational ensemble in QiRE is currently motivated conceptually rather than through a complete theoretical formalization, and the selection of its subspace dimension may require empirical adjustment across datasets. Moreover, as this is the first instance of applying such a structured probabilistic convolution, broader ablation studies will help further characterize its behavior and contribution relative to conventional stochastic or variational layers. These limitations do not fundamentally hinder the method but rather outline natural directions for continued development and validation.

Declaration of Competing Interest

The authors declare that they have no known competing financial interests or personal relationships that could have appeared to influence the work reported in this paper.

Authorship Contribution Statement

Amin Golnari: Conceptualization, Methodology, Software, Investigation, Visualization, Writing – Original Draft, Writing – Review & Editing. **Jamileh Yousefi:** Supervision, Validation, Writing – Review & Editing. **Reza Moheimani:** Investigation, Writing – Review & Editing. **Saeid Sanei:** Supervision, Validation, Formal Analysis, Writing – Review & Editing.

References

- [1] Yarin Gal and Zoubin Ghahramani. Dropout as a bayesian approximation: Representing model uncertainty in deep learning. pages 1050–1059, 2016.
- [2] Alex Kendall and Yarin Gal. What uncertainties do we need in bayesian deep learning for computer vision? *Advances in neural information processing systems*, 30, 2017.
- [3] Moloud Abdar, Farhad Pourpanah, Sadiq Hussain, Dana Rezazadegan, Li Liu, Mohammad Ghavamzadeh, Paul Fieguth, Xiaochun Cao, Abbas Khosravi, U Rajendra Acharya, et al. A review of uncertainty quantification in deep learning: Techniques, applications and challenges. *Information fusion*, 76:243–297, 2021.
- [4] Ranganath Krishnan and Omesh Tickoo. Improving model calibration with accuracy versus uncertainty optimization. *Advances in Neural Information Processing Systems*, 33:18237–18248, 2020.
- [5] Rohan Taori, Achal Dave, Vaishaal Shankar, Nicholas Carlini, Benjamin Recht, and Ludwig Schmidt. Measuring robustness to natural distribution shifts in image classification. *Advances in Neural Information Processing Systems*, 33:18583–18599, 2020.
- [6] Jun John Sakurai and Jim Napolitano. *Modern quantum mechanics*. Cambridge University Press, 2020.

- [7] Kerstin Beer, Dmytro Bondarenko, Terry Farrelly, Tobias J Osborne, Robert Salzmann, Daniel Scheiermann, and Ramona Wolf. Training deep quantum neural networks. *Nature communications*, 11(1):808, 2020.
- [8] Shaozhi Li, M Sabbir Salek, Binayak Roy, Yao Wang, and Mashrur Chowdhury. Quantum-inspired weight-constrained neural network: Reducing variable numbers by 100x compared to standard neural networks. *arXiv preprint arXiv:2412.19355*, 2024.
- [9] Shengyang Sun, Guodong Zhang, Jiaxin Shi, and Roger Grosse. Functional variational bayesian neural networks. *arXiv preprint arXiv:1903.05779*, 2019.
- [10] Saeid Sanei, Delaram Jarchi, and Anthony G Constantinides. *Body sensor networking, design and algorithms*. John Wiley & Sons, 2020.
- [11] Qinghao Zhao, Shijia Geng, Boya Wang, Yutong Sun, Wenchang Nie, Baochen Bai, Chao Yu, Feng Zhang, Gongzheng Tang, Deyun Zhang, et al. Deep learning in heart sound analysis: from techniques to clinical applications. *Health Data Science*, 4:0182, 2024.
- [12] Asmaa Ameen, Ibrahim Eldesouky Fattoh, Tarek Abd El-Hafeez, and Kareem Ahmed. Advances in ecg and pcg-based cardiovascular disease classification: a review of deep learning and machine learning methods. *Journal of Big Data*, 11(1):159, 2024.
- [13] Amit Krishna Dwivedi, Syed Anas Imtiaz, and Esther Rodriguez-Villegas. Algorithms for automatic analysis and classification of heart sounds—a systematic review. *IEEE Access*, 7:8316–8345, 2018.
- [14] Farhat Binte Azam, Md Istiaq Ansari, Shoyad Ibn Sabur Khan Nuhash, Ian McLane, and Taufiq Hasan. Cardiac anomaly detection considering an additive noise and convolutional distortion model of heart sound recordings. *Artificial Intelligence in Medicine*, 133:102417, 2022.
- [15] Tharindu Fernando, Harshala Gammulle, Simon Denman, Sridha Sridharan, and Clinton Fookes. Deep learning for medical anomaly detection—a survey. *ACM Computing Surveys (CSUR)*, 54(7):1–37, 2021.
- [16] Ahmed Barnawi, Mehrez Boulares, and Rim Somai. Simple and powerful pcg classification method based on selection and transfer learning for precision medicine application. *Bioengineering*, 10(3):294, 2023.
- [17] Umair Riaz, Sumair Aziz, Muhammad Umar Khan, Syed Azhar Ali Zaidi, Muhammad Ukasha, and Aamir Rashid. A novel embedded system design for the detection and classification of cardiac disorders. *Computational Intelligence*, 37(4):1844–1864, 2021.
- [18] Mike Schuster and Kuldip K Paliwal. Bidirectional recurrent neural networks. *IEEE transactions on Signal Processing*, 45(11):2673–2681, 1997.
- [19] Siddique Latif, Muhammad Usman, Rajib Rana, and Junaid Qadir. Phonocardiographic sensing using deep learning for abnormal heartbeat detection. *IEEE Sensors Journal*, 18(22):9393–9400, 2018.
- [20] Ehsanhosein Kalatehjari, Mohammad Mehdi Hosseini, Ali Harimi, and Vahid Abolghasemi. Advanced ensemble learning-based cnn-bilstm network for cardiovascular disease classification using ecg and pcg signal. *Biomedical Signal Processing and Control*, 108:107846, 2025.
- [21] Atitaya Phoemsuk and Vahid Abolghasemi. Enhanced coronary artery disease classification through feature engineering and one-dimensional convolutional neural network. *IEEE Access*, 2025.
- [22] Charles Blundell, Julien Cornebise, Koray Kavukcuoglu, and Daan Wierstra. Weight uncertainty in neural network. pages 1613–1622, 2015.
- [23] Christos Louizos and Max Welling. Multiplicative normalizing flows for variational bayesian neural networks. pages 2218–2227, 2017.
- [24] Turker Tuncer, Sengul Dogan, Ru-San Tan, and U Rajendra Acharya. Application of petersen graph pattern technique for automated detection of heart valve diseases with pcg signals. *Information Sciences*, 565:91–104, 2021.
- [25] Tien-En Chen, Shih-I Yang, Li-Ting Ho, Kun-Hsi Tsai, Yu-Hsuan Chen, Yun-Fan Chang, Ying-Hui Lai, Syu-Siang Wang, Yu Tsao, and Chau-Chung Wu. S1 and s2 heart sound recognition using deep neural networks. *IEEE Transactions on Biomedical Engineering*, 64(2):372–380, 2016.
- [26] Jay Karhade, Shaswati Dash, Samit Kumar Ghosh, Dinesh Kumar Dash, and Rajesh Kumar Tripathy. Time-frequency-domain deep learning framework for the automated detection of heart valve disorders using pcg signals. *ieee transactions on instrumentation and measurement*, 71:1–11, 2022.
- [27] Juwairiya Siraj Khan, Manoj Kaushik, Anushka Chaurasia, Malay Kishore Dutta, and Radim Burget. Cardi-net: A deep neural network for classification of cardiac disease using phonocardiogram signal. *Computer Methods and Programs in Biomedicine*, 219:106727, 2022.

- [28] Rakesh Chandra Joshi, Juwairiya Siraj Khan, Vinay Kumar Pathak, and Malay Kishore Dutta. Ai-cardiocare: artificial intelligence based device for cardiac health monitoring. *IEEE Transactions on Human-Machine Systems*, 52(6):1292–1302, 2022.
- [29] Ramith Hettiarachchi, Udith Haputhanthri, Kithmini Herath, Hasindu Kariyawasam, Shehan Munasinghe, Kithmin Wickramasinghe, Duminda Samarasinghe, Anjula De Silva, and Chamira US Edussooriya. A novel transfer learning-based approach for screening pre-existing heart diseases using synchronized ecg signals and heart sounds. In *2021 IEEE international symposium on circuits and systems (ISCAS)*, pages 1–5. IEEE, 2021.
- [30] Omair Rashed Abdulwareth Almanifi, Ahmad Fakhri Ab Nasir, Mohd Azraai Mohd Razman, Rabi Muazu Musa, and Anwar PP Abdul Majeed. Heartbeat murmurs detection in phonocardiogram recordings via transfer learning. *Alexandria Engineering Journal*, 61(12):10995–11002, 2022.
- [31] Ebrahim A Nehary and Sreeraman Rajan. Phonocardiogram classification by learning from positive and unlabeled examples. *IEEE Transactions on Instrumentation and Measurement*, 73:1–14, 2024.
- [32] Saeid Sanei, Tracey KM Lee, and Vahid Abolghasemi. A new adaptive line enhancer based on singular spectrum analysis. *IEEE Transactions on Biomedical Engineering*, 59(2):428–434, 2011.
- [33] Yuanyang Qi and Saeid Sanei. Murmur separation and classification from heart sound using constrained singular spectrum analysis and wavelet transform. In *2024 Asia Pacific Signal and Information Processing Association Annual Summit and Conference (APSIPA ASC)*, pages 1–5. IEEE, 2024.
- [34] Shichao Ma, Junyi Chen, and Joshua WK Ho. An edge-device-compatible algorithm for valvular heart diseases screening using phonocardiogram signals with a lightweight convolutional neural network and self-supervised learning. *Computer Methods and Programs in Biomedicine*, 243:107906, 2024.
- [35] Özkan Arslan. Automated detection of heart valve disorders with time-frequency and deep features on pcg signals. *Biomedical Signal Processing and Control*, 78:103929, 2022.
- [36] Han Li, Xinpei Wang, Changchun Liu, Qiang Zeng, Yansong Zheng, Xi Chu, Lianke Yao, Jikuo Wang, Yu Jiao, and Chandan Karmakar. A fusion framework based on multi-domain features and deep learning features of phonocardiogram for coronary artery disease detection. *Computers in biology and medicine*, 120:103733, 2020.
- [37] Khushbakht Iqtidar, Usman Qamar, Sumair Aziz, and Muhammad Umar Khan. Phonocardiogram signal analysis for classification of coronary artery diseases using mfcc and 1d adaptive local ternary patterns. *Computers in Biology and Medicine*, 138:104926, 2021.
- [38] Jorge Oliveira, Francesco Renna, Paulo Dias Costa, Marcelo Nogueira, Cristina Oliveira, Carlos Ferreira, Alípio Jorge, Sandra Mattos, Thamine Hatem, Thiago Tavares, et al. The circor digiscope dataset: from murmur detection to murmur classification. *IEEE journal of biomedical and health informatics*, 26(6):2524–2535, 2021.
- [39] Larry Huynh, Jin Hong, Ajmal Mian, Hajime Suzuki, Yanqiu Wu, and Seyit Camtepe. Quantum-inspired machine learning: a survey. *arXiv preprint arXiv:2308.11269*, 2023.
- [40] Richard Y Li, Sharvari Gujja, Sweta R Bajaj, Omar E Gamel, Nicholas Cilfone, Jeffrey R Gulcher, Daniel A Lidar, and Thomas W Chittenden. Quantum processor-inspired machine learning in the biomedical sciences. *Patterns*, 2(6), 2021.
- [41] Lu Bai, Luca Rossi, Lixin Cui, Jian Cheng, and Edwin R Hancock. A quantum-inspired similarity measure for the analysis of complete weighted graphs. *IEEE transactions on cybernetics*, 50(3):1264–1277, 2019.
- [42] Rajveer Singh Lalawat, Varun Bajaj, Prabin Kumar Padhy, and Chun-Yu Lin. Advancing motor imagery eeg classification by quantum feature integration and quantum support vector machines. *Applied Acoustics*, 240:110976, 2025.
- [43] Gunti Swathi, Ali Altalbe, and R Prasanna Kumar. Qucnet: quantum-inspired convolutional neural networks for optimized thyroid nodule classification. *IEEE Access*, 12:27829–27842, 2024.
- [44] Lubna Siddiqui, Ashish Mani, and Jaspal Singh. Towards quantum-inspired evolutionary algorithms for denoising pcg signals. pages 1–6, 2024.
- [45] Jinjing Shi, Tian Chen, Wei Lai, Shichao Zhang, and Xuelong Li. Pretrained quantum-inspired deep neural network for natural language processing. *IEEE Transactions on Cybernetics*, 54(10):5973–5985, 2024.
- [46] Ahmed Alamri, S Abdel-Khalek, Adel A Bahaddad, and Ahmed Mohammed Alghamdi. Innovative deep learning and quantum entropy techniques for brain tumor mri image edge detection and classification model. *Alexandria Engineering Journal*, 122:588–604, 2025.
- [47] Chao Ren, Rudai Yan, Huihui Zhu, Han Yu, Minrui Xu, Yuan Shen, Yan Xu, Ming Xiao, Zhao Yang Dong, Mikael Skoglund, et al. Toward quantum federated learning. *IEEE Transactions on Neural Networks and Learning Systems*, 2025.

- [48] D Banumathy, T Vetriselvi, K Venkatachalam, and Jaehyuk Cho. Quantum-inspired seagull optimised deep belief network approach for cardiovascular disease prediction. *PeerJ Computer Science*, 10:e2498, 2024.
- [49] Chengyu Liu, David Springer, Benjamin Moody, Ikaro Silva, Alistair Johnson, Maryam Samieinasab, Reza Sameni, Roger Mark, and Gari D Clifford. Classification of heart sound recordings-the physionet computing in cardiology challenge 2016. *PhysioNet*, 2016.
- [50] Jorge Oliveira, Francesco Renna, Paulo Costa, Marcelo Nogueira, Ana Cristina Oliveira, Andoni Elola, Carlos Ferreira, Alipio Jorge, Ali Bahrami Rad, Matthew Reyna, et al. The circor digiscope phonocardiogram dataset. In *IEEE Conference*, 2022.
- [51] Diederik P Kingma and Max Welling. Auto-encoding variational bayes. *arXiv preprint arXiv:1312.6114*, 2013.
- [52] Isis Didier Lins, Lavínia Maria Mendes Araújo, Caio Bezerra Souto Maior, Erico Souza Teixeira, Pâmela Thays Lins Bezerra, Márcio José das Chagas Moura, and Enrique López Droguett. Quantum-based optimization methods for the linear redundancy allocation problem: A comparative analysis. *Reliability Engineering & System Safety*, 262:111153, 2025.
- [53] Amin Golnari and Mostafa Diba. Adaptive real-time multi-loss function optimization using dynamic memory fusion framework: A case study on breast cancer segmentation. *Biomedical Signal Processing and Control*, 111:108388, 2026.
- [54] Amin Golnari, Mohammad Hossein Komeili, and Zahra Azizi. Probabilistic deep learning and transfer learning for robust cryptocurrency price prediction. *Expert Systems with Applications*, 255:124404, 2024.
- [55] Yi-Tang Hsieh, Hsien-Kuan Liu, Jiunn-Ren Wu, Ting-Yu Yan, Yu-Jung Huang, MeiHui Guo, and Ming-Chun Yang. Development and validation of an integrated residual-recurrent neural network model for automated heart murmur detection in pediatric populations. *Scientific Reports*, 15(1):19155, 2025.
- [56] Ahmed Patwa, Muhammad Mahboob Ur Rahman, and Tareq Y AI-Naffouri. Heart murmur and abnormal pcg detection via wavelet scattering transform & a 1d-cnn. *IEEE Sensors Journal*, 2025.
- [57] Fan Li, Hong Tang, Shang Shang, Klaus Mathiak, and Fengyu Cong. Classification of heart sounds using convolutional neural network. *Applied Sciences*, 10(11):3956, 2020.
- [58] Jehan Dastagir, Faiq Ahmad Khan, Muhammad Salman Khan, and Kaleem Nawaz Khan. Computer-aided phonocardiogram classification using multidomain time and frequency features. In *2021 International Conference on Artificial Intelligence (ICAI)*, pages 50–55. IEEE, 2021.
- [59] Ding Chen, Weipeng Xuan, Yexing Gu, Fuhai Liu, Jinkai Chen, Shudong Xia, Hao Jin, Shurong Dong, and Jikui Luo. Automatic classification of normal–abnormal heart sounds using convolution neural network and long-short term memory. *Electronics*, 11(8):1246, 2022.
- [60] Faiq Ahmad Khan, Anam Abid, and Muhammad Salman Khan. Automatic heart sound classification from segmented/unsegmented phonocardiogram signals using time and frequency features. *Physiological measurement*, 41(5):055006, 2020.
- [61] Palani Thanaraj Krishnan, Parvathavarthini Balasubramanian, and Snehalatha Umapathy. Automated heart sound classification system from unsegmented phonocardiogram (pcg) using deep neural network. *Physical and Engineering Sciences in Medicine*, 43(2):505–515, 2020.
- [62] Samit Kumar Ghosh, RN Ponnalagu, Rajesh Kumar Tripathy, Ganapati Panda, and Ram Bilas Pachori. Automated heart sound activity detection from pcg signal using time–frequency-domain deep neural network. *IEEE Transactions on Instrumentation and Measurement*, 71:1–10, 2022.
- [63] Daniel Enériz, Antonio J Rodriguez-Almeida, Himar Fabelo, Samuel Ortega, Francisco J Balea-Fernandez, Gustavo M Callico, Nicolás Medrano, and Belén Calvo. Low-cost fpga implementation of deep learning-based heart sound segmentation for real-time cvds screening. *IEEE Transactions on Instrumentation and Measurement*, 73:1–16, 2024.
- [64] Eduardo Soares, Plamen Angelov, and Xiaowei Gu. Autonomous learning multiple-model zero-order classifier for heart sound classification. *Applied Soft Computing*, 94:106449, 2020.
- [65] Yu-Yu Yen, Chun Chang, Jui-Hung Kao, and Woei-Chyn Chu. Development of a classification model for pediatric cardiac abnormality detection through the integration of child physiological data and phonocardiogram features. In *International Conference on Innovative Computing*, pages 81–90. Springer, 2025.
- [66] Omid Dehghan Manshadi and Sara Mihandoost. Murmur identification and outcome prediction in phonocardiograms using deep features based on stockwell transform. *Scientific Reports*, 14(1):7592, 2024.
- [67] Dixon Vimalajeewa, Chihoon Lee, and Brani Vidakovic. Multiscale analysis of heart sound signals in the wavelet domain for heart murmur detection. *Scientific Reports*, 15(1):10315, 2025.

- [68] Zixing Zhang, Tao Pang, Jing Han, and Björn W Schuller. Intelligent cardiac auscultation for murmur detection via parallel-attentive models with uncertainty estimation. In *ICASSP 2024-2024 IEEE International Conference on Acoustics, Speech and Signal Processing (ICASSP)*, pages 861–865. IEEE, 2024.
- [69] Truc Thi Kim Nguyen, Phuoc Nguyen Duy Vo, Tra Thi Bich Le, and Si Van Nguyen. Heart murmur classification using transfer learning and snapshot ensemble method. In *Proceedings of the 2024 9th International Conference on Intelligent Information Technology*, pages 454–459, 2024.
- [70] Yunendah Nur Fuadah, Muhammad Adnan Pramudito, and Ki Moo Lim. An optimal approach for heart sound classification using grid search in hyperparameter optimization of machine learning. *Bioengineering*, 10(1):45, 2022.